Contract N00014-83-K-0069

A CONCERTED TRIPLE DISSOCIATION - THE PHOTOCHEMISTRY OF S-TETRAZINE

Xinsheng Zhao, Walter B. Miller,*
Eric J. Hintsa, and Yuan T. Lee

Materials and Chemical Sciences Division,
Lawrence Berkeley Laboratory and
Department of Chemistry, University of California
Berkeley, California 94720, USA

Abstract

The method of photofragment-translational spectroscopy was used in a molecular beam study of the photochemistry of s-tetrazine. Following $^1B_{3u} \leftarrow {}^1A_g$ ($S_1 \leftarrow S_0$ excitation) or $^1B_{2u} \leftarrow {}^1A_g$ (248 nm excitation), s-tetrazine reverts to the highly vibrationally excited ground electronic state through internal conversion, then decomposes into 2HCN + N_2 via concerted triple dissociation. By analyzing the experimental data with a simple model, it was found that the potential energy surface along the reaction coordinate after the transition state is very repulsive, leading to most of the available energy, on average 73.9% in the case of $S_1 \leftarrow S_0$ excitation, going into translation. The asymptotic angles between N_2 and HCN with respect to the center-of-mass of s-tetrazine were 117.2 ± 0.5° and 114.4 ± 0.5° for $S_1 \leftarrow S_0$ and 248 nm excitation respectively.

I. Introduction

S-tetrazine (ST) is a member of the family of nitrogen containing compounds known as azines which are isoelectronic to each other and to benzene, and has long attracted attention from chemists due to its structure and properties. Since the pioneering work of Mason[1] and Spencer et al.,[2] this molecule has been intensively investigated and is now well understood spectroscopically in the neighborhood of the $^1A_g(S_0)$, $^1B_{3u}(S_1)$ and $^3B_{3u}(T_1)$ states.[3-9]

In contrast to the spectroscopy, a consensus has not been reached on the photochemistry of ST, as far as the dissociation mechanism is concerned.[3] Since an extensive review of the controversy over the suggested dissociation mechanism has been given in a recent publication by Scheiner and Schaefer (SS),[3] we will only emphasize a few important points.

While there is no doubt that the main outcome of $S_1 \leftarrow S_0$ excitation is dissociation, and that the products are HCN and N_2, different experiments support different mechanisms for the reaction

$$ST \xrightarrow{h\nu} 2HCN + N_2. \qquad (1)$$

In the case of the $S_1 \leftarrow S_0$ transition, the dissociation mechanisms can be classified into two categories.

Mechanism I: One photon absorption followed by internal conversion (IC) with dissociation occurring on the S_0 potential energy surface (PES), i.e.,

$$^1A_g\ ST \xrightarrow{h\nu} {}^1B_{3u}\ ST \xrightarrow{IC} [{}^1A_g\ ST]^{\ddagger} \rightarrow 2HCN + N_2 \qquad (2)$$

Within this scheme, concerted triple dissociation

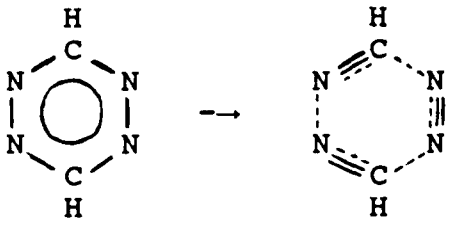

$$\rightarrow \qquad 2HCN + N_2 \qquad (3)$$

is the most plausible pathway.[10,11]

Mechanism II. Sequential two photon absorption followed by dissociation through an intermediate state other than the ground state:[12,13]

$$^1A_g\ ST \xrightarrow{h\nu} {}^1B_{3u}\ ST$$

$$\xrightarrow{h\nu} {}^1X\ ST$$

$$\rightarrow 2HCN + N_2, \qquad (4)$$

where ^1X is the intermediate state.

The strongest support for mechanism I to date is the theoretical calculation by Scheiner, Scuseria, and Schaefer (SSS).[10] Using standard double ζ and double ζ plus polarization basis sets, they carried out self-consistent field and configuration interaction calculations on ST. SSS were able to locate the transition state for triple dissociation on the S_0 PES, which is energetically accessible by $^1B_{3u} \leftarrow {}^1A_g$ excitation and leads to ground electronic state products. SS[3] also calculated the exothermicity of reaction (1). Fig. 1 presents an energy diagram according to the literature and the results of SS and SSS.

Support for mechanism II came from a molecular beam photofragmentation experiment by Glownia and Riley (GR).[14] In their experiment a molecular beam of ST from an effusive source (at 50°C) was irradiated in a vacuum chamber by a pulsed Nd:Yag laser at either the second harmonic (532 nm) or the fourth harmonic (266 nm) frequency. The most interesting result that GR obtained is that the time-of-flight (TOF) spectra of HCN at both laser wavelengths were almost identical, with an obvious bimodal shape. The spectrum of HCN contains a very fast narrow peak and a broad slow tail, while the TOF spectra of N_2 have only one component. Based on their analysis, GR argued for mechanism II with 532 nm excitation and assigned the intermediate state ^1X in reaction (4) as a $^1B_{2u}$ state, the same state reached by one photon excitation at 266 nm. GR argued further that the dissociation is a stepwise process:

$$ST \rightarrow HCNN_2 + HCN \rightarrow 2HCN + N_2. \qquad (5)$$

Faced with the inconsistencies between theory and experiment, a new experiment with better characterized experimental conditions has been carried out. As indicated by the title, our investigation has confirmed that s-tetrazine undergoes concerted triple dissociation, supporting the scheme of mechanism I. Furthermore, our results suggest that the photochemistry upon $^1B_{2u} \leftarrow {}^1A_g$ excitation follows the same route as with the $^1B_{3u} \leftarrow {}^1A_g$ transition.

It has been a challenge to analyze concerted triple dissociation product velocity and angular distributions

obtained in molecular beam experiments.[15-17] Recently, a concerted triple dissociation similar to reaction (3) was observed[17] where the three fragments were identical, so that the inherent three-fold symmetry allowed analysis to be carried out simply and accurately. For the analysis of the results obtained in this experiment and other molecular beam experiments where triple dissociation is involved, a simple general and realistic model is developed.

II. Experimental

The experimental apparatus has been described in detail elsewhere.[18] Briefly, a molecular beam and a laser beam were crossed at 90° in a vacuum chamber. Dissociation products passed through the aperture of the detector chamber at a variable angle with respect to the molecular beam. The neutral products were then ionized in an electron bombardment ionizer, mass selected by a quadrupole mass filter, and detected with a Daly-type ion counter. A multichannel scaler interfaced with an LSI-11 microcomputer recorded the arrival time of the signal relative to the laser pulse to obtain the TOF spectra. The distance between the interaction region and the ionizer is 36.7 cm. The angle between the molecular beam and the detector is variable between 0° and 90°, allowing us to detect even those products with very small center-of-mass (c.m.) translational energies. Installation of a liquid helium cooled cryopanel opposite the entrance slit to the detector not only greatly

reduces the background, but, more importantly, prevents dissociation products which scatter in the opposite direction to the detector from bouncing back into the detector to create false signal. In order to reduce the velocity spread of the ST beam and the chances of forming ST dimer, ST was held at 20 °C, He was used as a carrier gas with a total pressure of about 100 Torr, and the nozzle temperature was kept at 78 °C. With the above conditions the average beam velocity was 1.5×10^5 cm/sec with an 8% FWHM velocity spread.

For the excitation of the $^1B_{3u} \leftarrow ^1A_g$ transition, a Lambda Physik FL2002 dye laser was used with Coumarin 540A (Exciton), pumped by a Lambda Physik EMG 103 MSC excimer laser operated at 308 nm with a repetition rate of 100 Hz. The linewidth of the dye laser was about 0.2 cm^{-1}, and the laser was tuned to 18128.0 cm^{-1} for the 0-0 transition and 18830.9 cm^{-1} for the $6a_0^1$ transition.[5] A Glan-Taylor polarizer was used to obtain linearly polarized light in different directions. The laser beam was adjusted to a 1 mm diameter spot at the crossing point with the molecular beam.

To study the $^1B_{2u} \leftarrow ^1A_g$ transition, the same excimer laser was used with krypton fluoride at 248 nm, where the absorption of ST is almost at a maximum.[2] A MgF prism was used to separate the vertically and horizontally polarized laser beam, and the beam with the desired polarization was focused to 1 mm × 3 mm in the interaction region.

ST was synthesized according to the method given by

Spencer et al.[2] The precursor, s-tetrazine dicarboxylic acid, was made in advance and ST was prepared fresh from the precursor immediately before each experiment.

III. Results and analysis

A. General features

All the TOF spectra of mass-to-charge ratio (m/e) = 27 (HCN^+), two of which are shown in Fig. 2, and of m/e = 26 (CN^+), which are identical to that of m/e = 27, consist of a single fast sharp peak. TOF spectra of m/e = 28 (N_2^+) are also composed of only one peak, slightly broader and slower than that of the corresponding HCN, and two examples are also shown in Fig. 2. A search for fragments with m/e > 28 was carried out, but no signal was detected. The single fast peak in all the TOF spectra implies a one-step triple dissociation with large recoil velocity.

The TOF spectra due to excitation of two vibrational bands in the $^1B_{3u}\leftarrow{}^1A_g$ transition (hereafter 0-0 and $6a_0^1$ are used to stand for the respective bands of the $^1B_{3u}\leftarrow{}^1A_g$ transition) look the same. The peak positions in the TOF spectra of the products from 248 nm excitation are similar to those from $S_1\leftarrow S_0$ excitation, but the widths of the peaks are broader at 248 nm than that at $S_1\leftarrow S_0$ excitation. The polarization angle of the laser affects neither the signal level nor the shape of the TOF spectra much for HCN at all laser frequencies, but it does strongly affect the N_2 signal level at 248 nm.

At the normal output energy of the dye laser (about 10 mJ/pulse) the dissociation is highly saturated for both 0-0 and $6a_0^1$. In order to study the power dependence and to eliminate saturation effects, neutral density filters were placed in the path of the laser beam and the HCN fragment intensity was measured over a wide range of laser powers. The shape of the HCN TOF spectra was unchanged over the entire range. The dependence of the photolysis signal on the laser power for 0-0 plotted in Fig. 3 approaches linearity as the laser power approaches zero, providing unambiguous evidence that the dissociation of ST following $^1B_{3u} \leftarrow ^1A_g$ excitation is a one photon event.

The laser power dependence at 248 nm showed similar behavior, that is, saturation occurred at laser energies above 3 mJ/pulse, and the dependence approached linearity when the laser power was reduced below 3 mJ/pulse.

To prevent complications from saturation, the laser power was kept in the linear region when the laboratory angular dependence (varying the angle between the molecular beam and the detector) and laser polarization dependence (varying the angle between the electric vector of the laser and the detector) were measured for both 248 nm and $S_1 \leftarrow S_0$ excitation.

B. Simple model for analysis of triple dissociation

It is well known that in a two-body dissociation process momentum and energy conservation uniquely determine the relationship between the two fragments. When three particles

recoil from each other simultaneously, the situation becomes more complicated, because unless the three velocity vectors of the recoiling particles are measured simultaneously, it is difficult to get the translational energy distribution of the whole system from the measured individual velocity distributions of the fragments as can be done for two-body dissociation.

Consider a molecule simultaneously dissociating into particles 1, 2 and 3 with masses m_1, m_2 and m_3 respectively. A diagram of the dissociation process in velocity space is shown in Fig. 4, where $\hat{u}_1^0$, $\hat{u}_2^0$ and $\hat{u}_3^0$ are the direction vectors of the asymptotic velocities of particles 1, 2 and 3 in a body-fixed c.m. frame respectively, α and β are the angles between $\hat{u}_1^0$ and $\hat{u}_2^0$ and between $\hat{u}_1^0$ and $\hat{u}_3^0$ respectively, and $\delta = \pi-\alpha$ and $\gamma = \pi-\beta$. At this geometry the c.m. translational energy is

$$E_T = 1/2\ m_1(u_1^0)^2 + 1/2\ m_2(u_2^0)^2 + 1/2\ m_3(u_3^0)^2, \qquad (6)$$

and by momentum conservation,

$$m_2u_2^0\sin\delta = m_3u_3^0\sin\gamma$$
$$m_1u_1^0 = m_2u_2^0\cos\delta + m_3u_3^0\cos\gamma, \qquad (7)$$

where u_1^0, u_2^0 and u_3^0 are the magnitudes of the asymptotic velocities of the particles 1, 2 and 3 respectively.

If $\gamma+\delta \neq 0$, from (6) and (7) we have

$$E_T = \frac{m_1}{2}\left[1 + \frac{m_1}{\sin^2(\gamma+\delta)}\left(\frac{\sin^2\delta}{m_3} + \frac{\sin^2\gamma}{m_2}\right)\right](u_1^0)^2 . \qquad (8)$$

When $\gamma+\delta = 0$, the relation between E_T and u_1^0 becomes uncertain, but in the special situation when $u_2^0 = u_3^0$, the problem reduces

to a two-body problem corresponding to the dissociation of the molecule into m_1 and m_2+m_3, and the following equation can be used,

$$E_T = \frac{m_1}{2} \frac{m_1+m_2+m_3}{m_2+m_3}(u_1^0)^2, \qquad \gamma+\delta = 0. \tag{9}$$

If the molecule dissociates through only one asymptotic geometry, namely one set of α and β, the data analysis would be straightforward, using the method for two-body dissociation[19] with proper modification.

In a real system, although the angles α and β in individual dissociation events may vary, for a simultaneous triple dissociation the geometry must follow a certain distribution with respect to the two angles α and β as well as E_T, say, $F(\alpha,\beta;E_T)$. Therefore one way to approach the problem of data analysis is to find $F(\alpha,\beta;E_T)$ and to convolute the appropriate distribution.

In practice, however, there are some difficulties finding $F(\alpha,\beta;E_T)$: it does not treat the three particles equivalently. In the case where we do not know much about the structure and interaction potential of the transition state, we do not have any clue how $F(\alpha,\beta;E_T)$ will look, and it is not known whether $F(\alpha,\beta;E_T)$ is separable into $F(\alpha,\beta;E_T) = f(\alpha,E_T)g(\beta,E_T)$.

To avoid this problem we assume that at a fixed total internal energy there is a most probable dissociation geometry with reference angles α_r and β_r. We also assume that the distribution of geometries does not depend on the translational

energy and can be described by three factors which are functions of θ, η and ϕ respectively, i.e.,

$$G(\theta,\eta,\phi) = G_1(\theta)G_2(\eta)G_3(\phi) \quad , \tag{10}$$

where θ, η and ϕ are the angles between a particular asymptotic geometry of m_1, m_2 and m_3 and the most probable asymptotic geometry as shown in Fig. 4.

Since $G(\theta,\eta,\phi)$ treats the three particles independently and consists of distributions about the most probable values, we assume that the G_i's in equation (10) have the same mathematical form, and that Gaussian functions can be used as an approximation,

$$G_i(x) = A_i e^{-1/2(x/\sigma_i)^2} ; \quad i=1,2,3, \tag{11}$$

where A_i is a normalization factor and σ_i is a width parameter. Because it successfully fit the data, Eqn. (11) is the only functional form that we tried.

The angular distribution of the dissociation products for an electric dipole transition in a space-fixed c.m. coordinate frame has been expressed as[20,21]

$$P(\cos\Omega) = (1/4\pi)(1 + 2bP_2(\cos\Omega)) \quad , \tag{12}$$

where Ω is the polar angle of the direction of the fragments when the z axis is chosen along the electric field vector of the linearly polarized light, $P_2(x)$ is the second Legendre polynomial, and b is defined by

$$b = b'P_2(\cos\tau) \quad , \tag{13}$$

where τ is the angle between the transition dipole and the recoil velocity in a body fixed c.m. coordinate system, and b'

is a parameter which basically describes rotation and relaxation effects of the energized molecule. This interpretation has been rigorously verified for diatomic molecules.

For the triple dissociation of ST, let us consider that ST with a transition dipole along $\hat{\mu}$ absorbs a photon with electric field along $\hat{\epsilon}$. The absorption probability is proportional to $(\hat{\mu}\cdot\hat{\epsilon})^2$ in a classical picture, or in the conventional form

$$P_{abs}(\hat{\mu}\cdot\hat{\epsilon}) = (1/4\pi)(1+2P_2(\hat{\mu}\cdot\hat{\epsilon})), \qquad (14)$$

where $P_{abs}(\hat{\mu}\cdot\hat{\epsilon})$ is the angular distribution of absorption. After absorption the molecule can undergo a series of structural changes before it dissociates. We will assume that the lifetime of the molecule is long enough for the following discussion. Fig. 5 shows relevant relations, where $\mathbf{T}_0$ represents the direction from the c.m. of the molecule to the c.m. of the group of atoms which will be detected, at the moment of photon absorption, and $\mathbf{T}$ is the analogous direction at the transition state. Because the orientation of the molecules in space is isotropic, the initial directions of $\mathbf{T}_0$ which lead to the transition state along $\mathbf{T}$ are along circle 1 in Fig. 5. This means that the corresponding initial direction of the transition dipole μ is along circle 2, with θ_T the angle between μ and $\mathbf{T}$. The probability of a transition state along $\mathbf{T}$ is the average of equation (14) over circle 2, which is simply[22]

$$P_{\hat{\mathbf{T}}}(\hat{\mathbf{T}}\cdot\hat{\epsilon}) = (1/4\pi)(1+2P_2(\hat{\mu}\cdot\hat{\mathbf{T}})P_2(\hat{\mathbf{T}}\cdot\hat{\epsilon})) \ . \qquad (15)$$

If the asymptotic geometry is different from the transi-

tion state geometry, there is an angle between $\mathbf{T}$ and $\mathbf{u}^0$, the asymptotic velocity of the detected fragment in the body-fixed c.m. coordinate system. This difference is the result of intramolecular relaxation and internal motion near the transition state. The probability of a fragment along $\mathbf{u}^0$ is (15) averaged over circle 3, which is

$$P_{\hat{\mathbf{u}}^0}(\hat{\mathbf{u}}^0\cdot\hat{\epsilon}) = (1/4\pi)(1+2P_2(\hat{\mu}\cdot\hat{\mathbf{T}})P_2(\hat{\mathbf{T}}\cdot\hat{\mathbf{u}}^0)P_2(\hat{\mathbf{u}}^0\cdot\hat{\epsilon})). \qquad (16)$$

The physical basis of Eqn. (16) is that molecular rotation and internal motion of the molecule cause randomization of the direction of the tangential component of the fragment recoil velocity. This is an implicit effect which makes the average along circle 3 valid and is not directly reflected in the formula. In general, the magnitude of $P_2(\hat{\mathbf{T}}\cdot\hat{\mathbf{u}}^0)$ is different for each individual fragment, and we call it the local anisotropy parameter. Then, as in previous papers[20,21] we introduce the parameter b_1 to account for the smearing out effect of molecular rotation on the angular distribution of the photofragment in a space-fixed frame, which we call the direct effect of molecular rotation on the anisotropy. Mathematically, b_1 is the result of the transformation of the c.m. coordinate system from the body-fixed frames to the space-fixed frame, summed over all possible relations between the different frames. Therefore, the photofragment c.m. angular distribution in the space-fixed frame is

$$P_{\hat{\mathbf{u}}}(\hat{\mathbf{u}}\cdot\hat{\epsilon}) = (1/4\pi)(1+2b_1P_2(\hat{\mu}\cdot\hat{\mathbf{T}})P_2(\hat{\mathbf{T}}\cdot\hat{\mathbf{u}}^0)P_2(\hat{\mathbf{u}}\cdot\hat{\epsilon})), \qquad (17)$$

where $\hat{\mathbf{u}}$ is the unit vector of the asymptotic c.m. velocity of

the fragment in the space-fixed frame. According to the above physical and mathematical explanations, b_1 is the same for all the fragments, and we call b_1 the global anisotropy parameter. It is emphasized that where the implicit effect of molecular rotation is important, Eqn. (17) reveals information about the geometry of the transition state. By measuring the laboratory angular dependence and/or laser polarization dependence, θ_T can be obtained within the above approximation.

Obviously, there is a distribution between $\mathbf{u}^0$ and $\mathbf{T}$, and according to our approximation it is related to $G(\theta,\eta,\phi)$ of Eqn. (10). Therefore, to get the overall probability of signal at direction $\hat{\mathbf{u}}$, Eqn. (17) should be averaged over the distribution function (10). Since the further derivation to obtain the TOF distribution is similar to that for two-body dissociation which is presented elsewhere,[19] only the final formula is given,

$$N^+_{m1,lab}(t,\omega_D) = C^+_{m1}\frac{v_1^2}{t}\int \lambda\frac{P_E(E_T)}{u_1} P_{\hat{\mathbf{u}}}(\hat{\mathbf{u}}_1\cdot\hat{\epsilon})\cdot N_B(V_B,\omega_B)G(\theta,\eta,\phi)\,dV_B d\omega_B d\theta d\eta d\phi d\omega_{m1}, \qquad (18)$$

where $N^+_{m1,lab}(t,\omega_D)$ is the calculated TOF spectrum of ion signal from m_1, t is the arrival time, ω_D is the detector solid angle, v_1 and u_1 are the laboratory and c.m. velocities of m_1 respectively, C^+_{m1} is a constant for each m/e, $P_E(E_T)$ is the product c.m. translational energy distribution, $N_B(V_B,\omega_B)$ is the reactant laboratory velocity distribution as a function of the velocity V_B and solid angle ω_B of the molecular beam, ω_{m1}

is the laboratory solid angle of m_1 in velocity space, and

$$\lambda = m_1\left[1 + \frac{m_1}{\sin^2(\delta+\gamma)}\left(\frac{\sin^2\delta}{m_3} + \frac{\sin^2\gamma}{m_2}\right)\right], \quad \delta+\gamma \neq 0;$$

$$= m_1\frac{m_1+m_2+m_3}{m_2+m_3}, \quad \delta+\gamma = 0. \tag{19}$$

C. Analyzed results

a. $S_1 \leftarrow S_0$ excitation

After the above discussion we can start to analyze the data using the triple dissociation mechanism. Since the $^1B_{3u} \leftarrow {}^1A_g$ transition dipole is perpendicular to the molecular plane, it must also be perpendicular to the recoil directions of all the fragments at the transition state, provided that the transition state is planar, as has been calculated by SSS.[10] As mentioned before, at the $S_1 \leftarrow S_0$ transition the dependence of the signal on the laser polarization angle is very weak, indicating that the lifetime of the energized molecule is much longer than its rotational period. From this fact we can immediately conclude that the absolute value of the global anisotropy parameter b_1, which is the same for both HCN and N_2, is very small, and the data is not sensitive to the geometry of the transition state. We did not collect any angular or polarization dependence data for N_2, because it would not provide any more information and the detection of N_2 is much more difficult due to high detector background.

Testing different sets of parameters, we found that the

peak positions in the TOF spectra are very sensitive to α_r and β_r. Although the TOF spectra of N_2 do not have good signal-to-noise, it was found that in order to fit all the TOF spectra, the deviation in α_r and β_r must be less than 0.5° from the best values. Setting all the σ_i to the same value, within the range $0 \leq \sigma_i \leq 5.2°$, it was always possible to fit the data by adjusting the translational energy distribution, $P_E(E_T)$. But if the constraint of maximum translational energy (E_{max}) is imposed, both the $P_E(E_T)$ and σ_i are uniquely determined within experimental error. For example, at a given E_{max} the σ_i has uncertain within ±0.2°. The high sensitivity of the fit to α_r, β_r and σ_i provides a sensitive probe of the detailed dissociation dynamics.

The exothermicity of reaction (1) is not experimentally known, although there are some estimates and theoretical calculations.[3,23] The theoretical prediction given by SS^3 is 57.4 kcal/mol, which should be within a few kcal/mol of the true value. From this experiment an accurate value for the exothermicity of reaction (1) cannot be obtained due to the fact that E_{max} and σ_i are correlated, but in order to fit the data the exothermicity of the reaction must range between 47.5 and 68.3 kcal/mol, which correspond to σ_i = 5.2° and 0° respectively, if the E_{max} corresponds to all the available energy in translation.

With the exothermicity given by SS, a set of parameters was obtained by fitting the experimental TOF spectra and is

listed in Table 1. Examples of the fits of the individual TOF spectra are given in Fig. 2. The $P_E(E_T)$ to fit the $6a_0^1$ data is plotted as curve (a) in Fig. 6. Fig. 7 shows the laser polarization dependence of HCN at a laboratory angle of 20°. The b_1 value obtained is in the range from 0 to 0.13. The near zero value of b_1 is a reflection of the near isotropic dissociation.

The immediate conclusion from Fig. 6 is that most of the available energy is channeled into translation in the $^1B_{3u} \leftarrow ^1A_g$ transition. This is in good agreement with the observation by Coulter et al.[24] that the population of products excited in the stretching modes is low. The average translational energy from $6a_0^1$ excitation is 82.2 kcal/mol, which is 73.9% of the total available energy of 111.2 kcal/mol, implying a very repulsive PES along the reaction coordinate after the transition state. Data from $6a_0^1$ and 0-0 give the same information except that E_{max} is adjusted correspondingly.

b. 248 nm excitation

At 248 nm, the transition is $^1B_{2u} \leftarrow ^1A_g$ and the transition dipole is along the y axis of the molecule (see Fig. 5 for the definition of the coordinates). The situation concerning anisotropy of different fragments is more interesting than in the case of the $S_1 \leftarrow S_0$ transition , and we observed different polarization dependence for HCN and N_2, as shown in Table 2.

At 248 nm it was impossible to simultaneously fit the TOF spectra of HCN and N_2 assuming the same σ_i for both the fragments. Although the peaks in the TOF spectra do not change

very much between 248 nm and $S_1 \leftarrow S_0$ excitation, the α_r and β_r derived from the data are noticeably different for the two wavelengths. The parameters which give the best fit are listed in Table 1 and examples of the fits to the individual spectra are shown in Fig. 2. The $P_E(E_T)$ used to fit the data is presented as curve (b) in Fig. 6.

Comparing the two $P_E(E_T)$'s in Fig. 6, it can be seen that the energy distribution at 248 nm is much broader than that from $S_1 \leftarrow S_0$ excitation. However, even though the photon energy at 248 nm is more than twice that of $S_1 \leftarrow S_0$ excitation, the energies of the peaks of the $P_E(E_T)$'s are similar. The average translational energy release at 248 nm excitation is 96.2 kcal/mol or 55.8% of the available energy, 172.4 kcal/mol. The similarity of the peak translational energies at both 248 nm and $S_1 \leftarrow S_0$ excitation is a very important phenomenon which will be discussed later.

Simulating the experimental results with the above model, we found that the fit to the individual TOF spectra does not depend strongly on information concerning the transition state, but because for 248 nm excitation the transition dipole is in the plane of the molecule and since the signal level strongly correlates with the laser polarization angle, the laser polarization dependence is very sensitive to the angle θ_T. For N_2 we set θ_T to 0°, since if the change in geometry leading to the transition state is defined within C_{2v} symmetry (correct according to SSS[10]), the N_2 must remain aligned in the direc-

tion of μ in the body-fixed c.m. frame. Therefore, from the fit to the N_2 data, $b_1 = 0.65 \pm 0.05$ in Eqn. (17) is obtained first, which we assume to be the same for HCN. Then we use this b_1 to fit all the HCN data by adjusting θ_T for HCN which is also the angle between the HCN and N_2 groups at the transition state. By this procedure, a value of $121.3 \pm 1°$ for θ_T is obtained. The laboratory angular distributions of HCN for both horizontally and vertically polarized light are plotted in Fig. 8. Similar to Fig. 7, the signal-to-noise ratio in Fig. 8 is not very satisfactory, since the laser power was set low to avoid saturation and the molecular beam density was rather low due to the low vapor pressure of ST. Long time averaging at one time is impossible due to the small amounts of ST obtained in each batch.

IV. Discussion

Using our model, the experimental data are successfully interpreted by concerted triple dissociation (TD). However, we would like to determine the boundary between TD and two-body sequential dissociation (SD), since at the limit of an infinitesimal interval between the primary and secondary steps of SD, TD and SD both offer the same physical picture.

Attempts were made to fit the data as a process involving secondary dissociation,[17,19] although we did not find any signal for the intermediates of either reaction (5) or (20).

$$ST \rightarrow N_2 + HCNNCH \rightarrow N_2 + 2HCN \ . \qquad (20)$$

These attempts were all unsuccessful for a variety of reasons, such as the trial distributions being unphysical, the distributions which fit one fragment could not fit its counterpart, or the simulated laboratory angular distribution or polarization dependence did not agree with the experimental results. Our conclusion is that neither reaction (5) nor (20) is consistent with our observations.

In fact, reaction (5) can easily be rejected, because we would expect to see two different kinds of HCN fragments, but the results do not show this at all. Reaction (20) must be considered more carefully. In our experimental set up, if every dissociation event maintains C_{2v} symmetry, TD is equivalent to SD with the constraint that secondary dissociation occurs only in a direction perpendicular to the primary recoil velocity and the primary and secondary E_T's are strongly correlated with each other.

Using mechanism (20), the TOF spectra of N_2 were fit first to obtain a primary $P_E(E_T)$ and an anisotropy parameter b_1. With those, the HCN TOF spectra were then fit by adjusting the secondary $P_E(E_T)$ and c.m. angular distribution.

For 0-0 and $6a_0^1$, it was possible to fit all the data this way. In Fig. 9 the secondary c.m. angular distribution which fits the $6a_0^1$ data is presented, where the distribution was made as broad as possible using the narrowest possible secondary $P_E(E_T)$ for the purpose of the following argument. The secondary products are sharply distributed perpendicular to the

primary velocity vector, implying that the secondary process in the SD scheme is strongly correlated to the primary process. If we assume that all the secondary recoil events occurred perpendicular to the primary recoil direction, and that the width of the secondary angular distribution in Fig. 9 was due only to the rotation of HCNNCH, we can estimate the time, Δt, from the start of the primary recoil to the end of the secondary recoil, and estimate how far the fragments would fly away from each other during this time assuming that they had reached their asymptotic velocity. Δt is estimated to be 0.3 psec, with a displacement within a few angstroms. The values estimated above are rather crude, but in any event the time and distance are so short that it is inappropriate to consider the process separated in the sense of SD. Moreover, because the bond energy of any bond in ST is expected to be much higher than the $6a_0^1$ photon energy of 53.8 kcal/mol, SD is energetically unlikely for $S_1 \leftarrow S_0$ excitation.

For 248 nm excitation, the data cannot be fit using mechanism (20). We can fit the TOF spectrum of HCN at one laboratory angle and one polarization angle by the same method as above, but it is impossible to simulate the TOF spectra at all angles using the same set of parameters. The calculated laboratory angular distribution and laser polarization dependence of the signal just did not agree with the experimental results, because of the observed anisotropy which is different from that for $S_1 \leftarrow S_0$ excitation.

According to SSS's orbital correlation diagram[10] neither $^1B_{2u}$ nor $^1B_{3u}$ correlate adiabatically with the product ground states if C_{2v} symmetry is maintained throughout dissociation. As shown in Fig. 1, the energy of the $S_1 \leftarrow S_0$ transition is lower than the energy required to populate the lowest excited (singlet) states of the products, so that it is impossible to produce electronically excited product molecules. It has been reported[25] that the rate of relaxation from the S_1 state is 10^5 times that from the T_1 state. Therefore, the path of dissociation after intersystem crossing is not important and the dissociation must occur on the S_0 PES after IC. Experiments as well as theory show[3,9,26] that there is strong interaction between the S_0 and S_1 electronic states and that IC is the main deactivation pathway for S_1. Combined with the previous studies, our experiment provides convincing evidence for the mechanism described by equations (2) and (3).

We have found no other experimental studies of the photochemistry of $^1B_{2u} \leftarrow ^1A_g$ except that of GR. The energy at 248 nm is high enough to allow one of the HCN molecules to be electronically excited. As shown in Fig. 6, the minimum translational energy released in 248 nm photolysis is 37.0 kcal/mol. Even if all the remaining energy went into electronic excitation, it would still be 13.6 kcal/mol less than that needed to reach the first excited singlet state of HCN. Therefore, it is almost certain that no electronically excited products are formed at 248 nm either. Since the $^1B_{2u}$ state does not

correlate with ground state products, it is unlikely that the dissociation is directly from $^1B_{2u}$ reactant to products, even though calculations predict that there should be two imaginary vibrational modes on the $^1B_{2u}$ PES within the constraint of D_{2h} symmetry.[3] As pointed out in many previous studies,[17,27-29] the translational energy release mainly correlates with the exit barrier along the reaction coordinate and is less influenced by the excess energy when there is an appreciable exit barrier. If both dissociation processes occur on the S_0 PES and the S_0 lifetime is long enough to allow substantial intramolecular vibrational redistribution, the peak positions of the $P_E(E_T)$'s should be similar, because the fragments experience the same exit barrier. The excess energy is mainly distributed throughout all the internal modes (including the reaction coordinate). Thus, the most obvious difference between different internal energies for the same transition state is that the higher the energy the broader the distribution, while the change in the peak position will be much smaller than the change in the excess energy. Applying this idea to ST, it is obvious that the dissociation dynamics following the two electronic excitation are qualitatively very similar. Further evidence is that the angle between N_2 and HCN at the transition state is 121.3 ± 1° at 248 nm, which is fairly close to 120.1°, the value calculated from the transition state geometry provided by SSS.[10] Therefore, we suggest that the dissociation mechanism following $^1B_{2u} \leftarrow ^1A_g$ excitation

is the same as that for $^1B_{3u} \leftarrow {}^1A_g$ excitation, i.e., IC to ground state ST and triple dissociation to ground state products.

The parameter b_1 gives an idea of how fast dissociation occurs with respect to the rotational period. For $S_1 \leftarrow S_0$ excitation, $b_1 \leq 0.13$ implies that dissociation is much slower than the rotational period of the parent molecule. For 248 nm excitation, $b_1 = 0.65$ indicates that the products still have a strong "memory" of the initial orientation, implying that the dissociation lifetime following $^1B_{2u} \leftarrow {}^1A_g$ excitation is comparable to or less than the rotational period. Assuming that RRKM theory[30] is applicable in predicting rate constants for triple dissociation, we can use a reasonable set of vibrational frequencies[31] and the potential barrier (shown in Fig. 1) given by SSS[10] to estimate the RRKM dissociation lifetime. Our calculation gives RRKM dissociation lifetimes for triple dissociation of 50 nsec and 0.2 psec for 0-0 and 248 nm excitation respectively. Although a lifetime of 0.2 psec is questionable because RRKM theory may not be valid on such a short timescale, the predicted lifetime for 0-0 transition is reasonable. The fluorescence lifetime from the S_1 state has been measured to be on the order of 0.1 - 1 nsec.[7] Thus, the molecule has plenty of time to randomize its energy after IC in the case of $S_1 \leftarrow S_0$ excitation. At 248 nm, the value of b_1 implies that IC rate is probably on the same order of magnitude as that of dissociation after IC.

It is instructive to compare the geometry change through

the dissociation. The angles between the HCN and N_2 groups for the most probable asymptotic geometries at 248 nm and $S_1 \leftarrow S_0$ excitation and the geometry of the transition state obtained in this experiment are 114.4°, 117.2°, and 121.3° respectively. The asymptotic angles are smaller than at the transition state, and the higher the available energy the smaller the angle, which implies that the repulsion between two HCN is stronger than that between HCN and N_2 during the process of the molecule breaking the conjugated π-σ bond system. Comparison of σ_i between the two laser wavelengths (in Table 1) indicates that at 248 nm, because of the higher available energy, the molecule can dissociate from configurations which deviate more from the lowest energy ST structure, and the dissociation becomes more asymmetric. These observations are consistent with our intuition and provide a vivid picture of the dynamics of ST triple dissociation.

V. Conclusions

This experimental study has confirmed that the s-tetrazine photodissociation is a concerted triple dissociation. To analyze the experimental results, a simple model is proposed which has proven to be fruitful and sensitive to the experimental data. It is found that information on both the detailed dissociation dynamics and the transition state can be derived in certain systems using this model. An improved analysis of the physical significance of the anisotropy parameter is given,

where the relation between the anisotropy parameter and the geometry of the transition state is explicitly constructed.

Acknowledgements

The authors wish to thank A. C. Scheiner and H. F. Schaefer III for providing their results prior to publication, and X. Z. thanks A. C. Scheiner for helpful discussions. This work was supported by the Office of Naval Research under contract No. N00014-83-K-0069.

References

* Permanent address: Department of Chemistry, University of Arizona, Tucson, Arizona 85721.

1. S. F. Mason, J. Chem. Soc. (London) 1263, 1269 (1959).
2. G. H. Spencer Jr., P. C. Cross, and K. B. Wiberg, J. Chem. Phys. **35**, 1925, 1939 (1961).
3. A. C. Scheiner and H. F. Schaefer III, J. Chem. Phys. **87**, 3539 (1987), and references therein.
4. K. K. Innes, J. P. Byrne, and I. G. Ross, J. Mol. Spectrosc. **22**, 125 (1967), and references therein.
5. K. K. Innes, L. A. Franks, A. J. Merer, G. K. Vemulapalli, T. Cassen, and J. Lowry, J. Mol. Spectrosc. **66**, 465 (1977).
6. D. V. Brumbaugh and K. K. Innes, Chem. Phys. **59**, 413 (1981).
7. D. V. Brumbaugh, C. A. Haynam, and D. H. Levy, J. Mol. Spectrosc. **94**, 316 (1982).
8. K. B. Thakur, V. A. Job, and V. B. Kartha, J. Mol. Spectrosc., a) **107**, 373 (1984), b) **112**, 340 (1985).
9. A. Kiermeier, K. Dietrich, E. Riedle, and H. J. Neusser, J. Chem. Phys. **85**, 6983 (1986).
10. A. C. Scheiner, G. E. Scuseria, and H. F. Schaefer III, J. Am. Chem. Soc. **108**, 8160 (1986).
11. D. S. King, C. T. Denny, R. M. Hochstrasser, and A. B. Smith III, J. Am. Chem. Soc. **99**, 271 (1977).
12. D. M. Burland, F. Carmona, and J. Pacansky, Chem. Phys.

Lett. **56**, 221 (1978).

13. M. Paczkowski, R. Pierce, A. B. Smith III, and R. M. Hochstrasser, Chem. Phys. Lett. **72**, 5 (1980).
14. J. H. Glownia and S. J. Riley, Chem. Phys. Lett. **71**, 429 (1980).
15. P. M. Kroger and S. J. Riley, J. Chem. Phys. **70**, 3863 (1979).
16. J. W. Hepburn, R. J. Buss, L. J. Butler, and Y. T. Lee, J. Phys. Chem. **87**, 3638 (1983).
17. X. Zhao, E. J. Hintsa, and Y. T. Lee, J. Chem. Phys. **88**, 801 (1988).
18. A. M. Wodtke and Y. T. Lee, J. Phys. Chem. **89**, 4744 (1985).
19. X. Zhao, G. M. Nathanson, and Y. T. Lee, to be published.
20. R. N. Zare, Mol. Photochem. **4**, 1 (1972).
21. G. E. Busch and K. R. Wilson, J. Chem. Phys. **56**, 3638 (1972).
22. To obtain equations (15) and (16), the addition theorem of Legendre functions was used.
23. M. J. S. Dewar, Pure Appl. Chem. **44**, 767 (1975).
24. D. Coulter, D. Dows, H. Reisler, and C. Wittig, Chem. Phys. **32**, 429 (1978).
25. R. M. Hochstrasser and D. S. King, J. Am. Chem. Soc. **97**, 4760 (1975).
26. a) V. L. Windisch, A. B. Smith III, and R. M. Hochstrasser, J. Phys. Chem. **92**, 5366 (1988); b) K. K. Innes, J.

Chem. Phys. **76**, 2100 (1982).

27. D. Krajnovich, F. Huisken, Z. Zhang, Y. R. Shen, and Y. T. Lee, J. Chem. Phys. **77**, 5977 (1982).

28. L. J. Butler, R. J. Buss, R. J. Brudzynski, and Y. T. Lee, J. Phys. Chem. **87**, 5106 (1983).

29. A. M. Wodtke, E. J. Hintsa, and Y. T. Lee, J. Phys. Chem. **90**, 3549 (1986).

30. P. J. Robinson and K. A. Holbrook, Unimolecular Reactions, Wiley, London (1972).

31. The calculated vibrational frequencies for the transition state were kindly provided by A. C. Scheiner. For consistency, the theoretically predicted vibrational frequencies for "stable" ST in ref. 3 were used in the RRKM calculation.

Table 1. Parameters derived from data analysis

	α_r(HCN,HCN)	α_r(HCN,N_2)	σ(HCN)	σ(N_2)
$S_1 \leftarrow S_0$	125.7°	117.2°	4.4°	4.4°
248 nm	131.2°	114.4°	8.5°	9.0°

	b_1	θ_T(HCN)	θ_T(N_2)
$S_1 \leftarrow S_0$	≤0.13	90°	90°
248 nm	0.65	121.3°	0°

Table 2. Laser polarization dependence for 248 nm excitation at 20°

Laser polarization	Signal Counts HCN	N_2
Vertical[a]	1.00	1.00
Horizontal	0.84	4.52

a Set to 1.00.

Figure captions

Fig. 1 Energy diagram of ST photodissociation with energies in kcal/mol.

Fig. 2 TOF spectra at a laboratory angle of 20°. The scattered circles are the experimental data and the solid lines are the fits with the triple dissociation mechanism. The TOF spectra shown for $6a_0^1$ ($^1B_{3u} \leftarrow {}^1A_g$) excitation were taken using vertically polarized light, and for 248 nm excitation horizontally polarized light was used.

Fig. 3 Laser power dependence of the HCN signal for the 0-0 ($^1B_{3u} \leftarrow {}^1A_g$) transition at 20° with the laser vertically polarized.

Fig. 4 Asymptotic geometry in velocity space for triple dissociation. $\hat{u}_1^0$, $\hat{u}_2^0$ and $\hat{u}_3^0$ are the unit recoil velocity vectors in a particular dissociation event, while $\hat{u}_1^r$, $\hat{u}_2^r$ and $\hat{u}_3^r$ are the reference velocity vector corresponding to the most probable dissociation geometry. The other variables are explained in the text.

Fig. 5 Diagram of the relations between fragments from photon absorption, through the transition state, to the asymptotic geometry. The direction of the transition dipole μ in the figure corresponds to the

case of $^1B_{2u} \leftarrow ^1A_g$ UV excitation. All symbols are explained in the text.

Fig. 6 Triple dissociation $P_E(E_T)$'s used to fit the data. Curve (a) is for $6a_0^1$ ($^1B_{3u} \leftarrow ^1A_g$) excitation, and curve (b) is for 248 nm excitation.

Fig. 7 Polarization dependence of HCN signal for the 0-0 ($^1B_{3u} \leftarrow ^1A_g$) transition at a laboratory angle of 20°. Points are experimental data and the line is the fit using $b_1 = 0.13$ and other parameters in Table 1. If $b_1 = 0$, the fit would be a horizontal straight line.

Fig. 8 Laboratory angular distribution of HCN at 248 nm. Points are experimental data and the lines are the fits using the parameters in Table 1. V and H stand for vertically and horizontally polarized laser beams respectively. For an isotropic product distribution, the two lines would be identical.

Fig. 9 The secondary c.m. angular distribution of HCN used to fit the $6a_0^1$ ($^1B_{3u} \leftarrow ^1A_g$) data by sequential reaction mechanism (20), where 0° corresponds to the direction of the primary recoil vector of $H_2C_2N_2$.

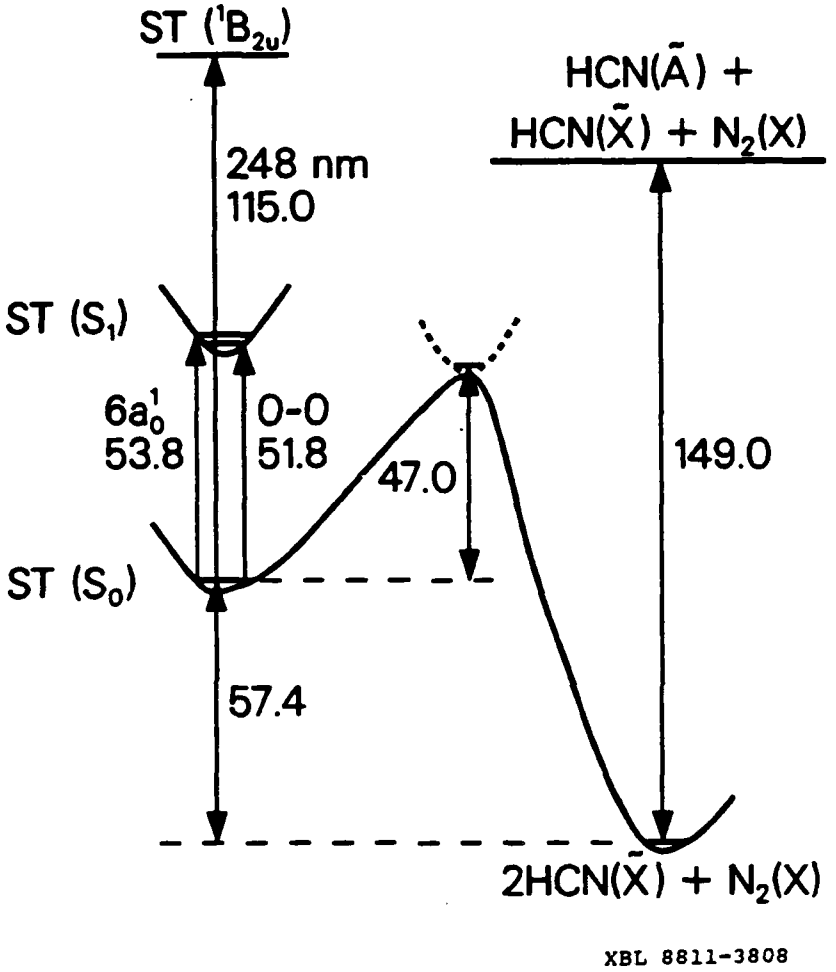
ST ($^1B_{2u}$)
HCN(Ã) +
HCN(X̃) + N_2(X)
248 nm
115.0
ST (S_1)
$6a_0^1$
53.8
0-0
51.8
47.0
149.0
ST (S_0)
57.4
2HCN(X̃) + N_2(X)
XBL 8811-3808

Fig 1

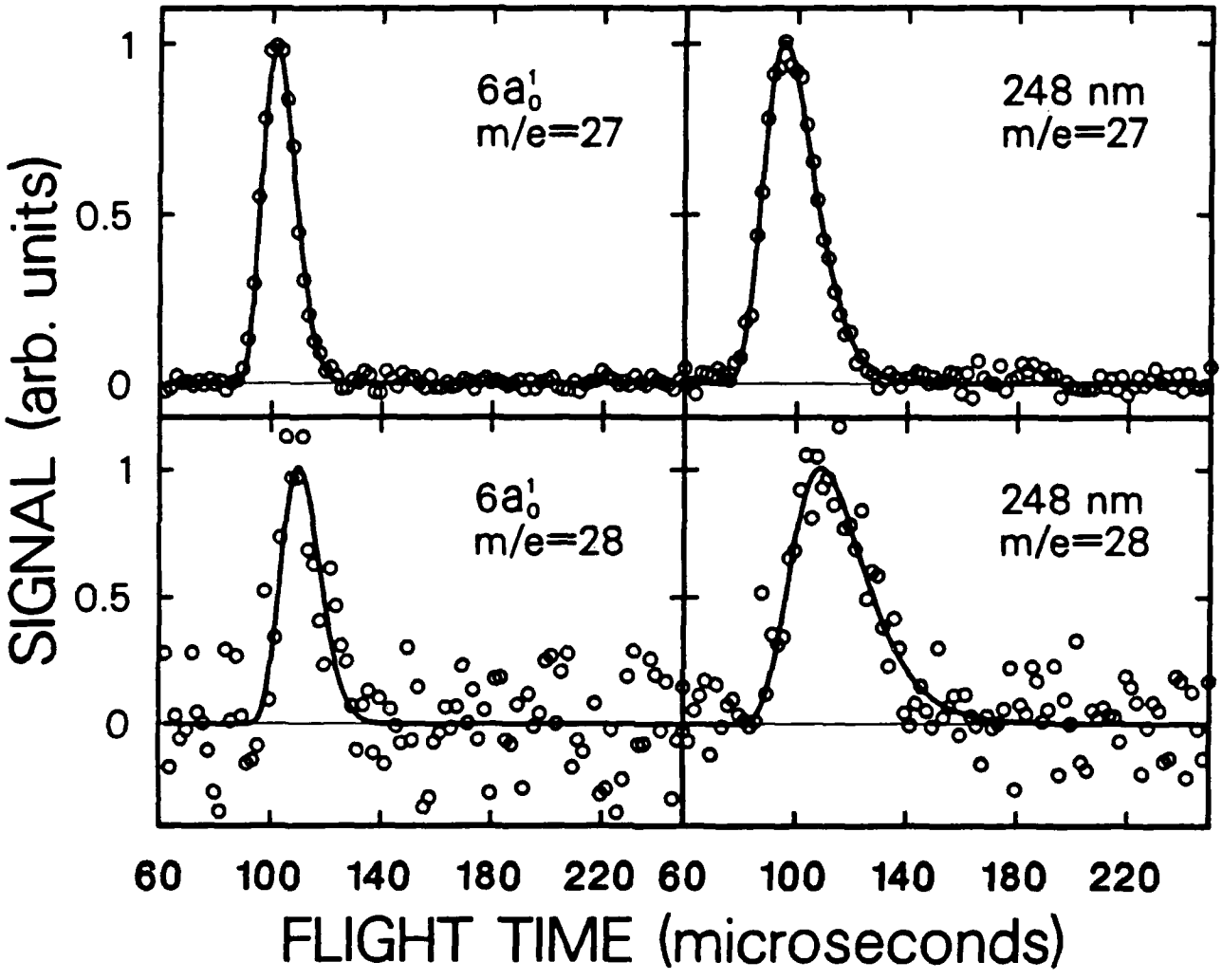

XBL 8811-3807

Fig 2

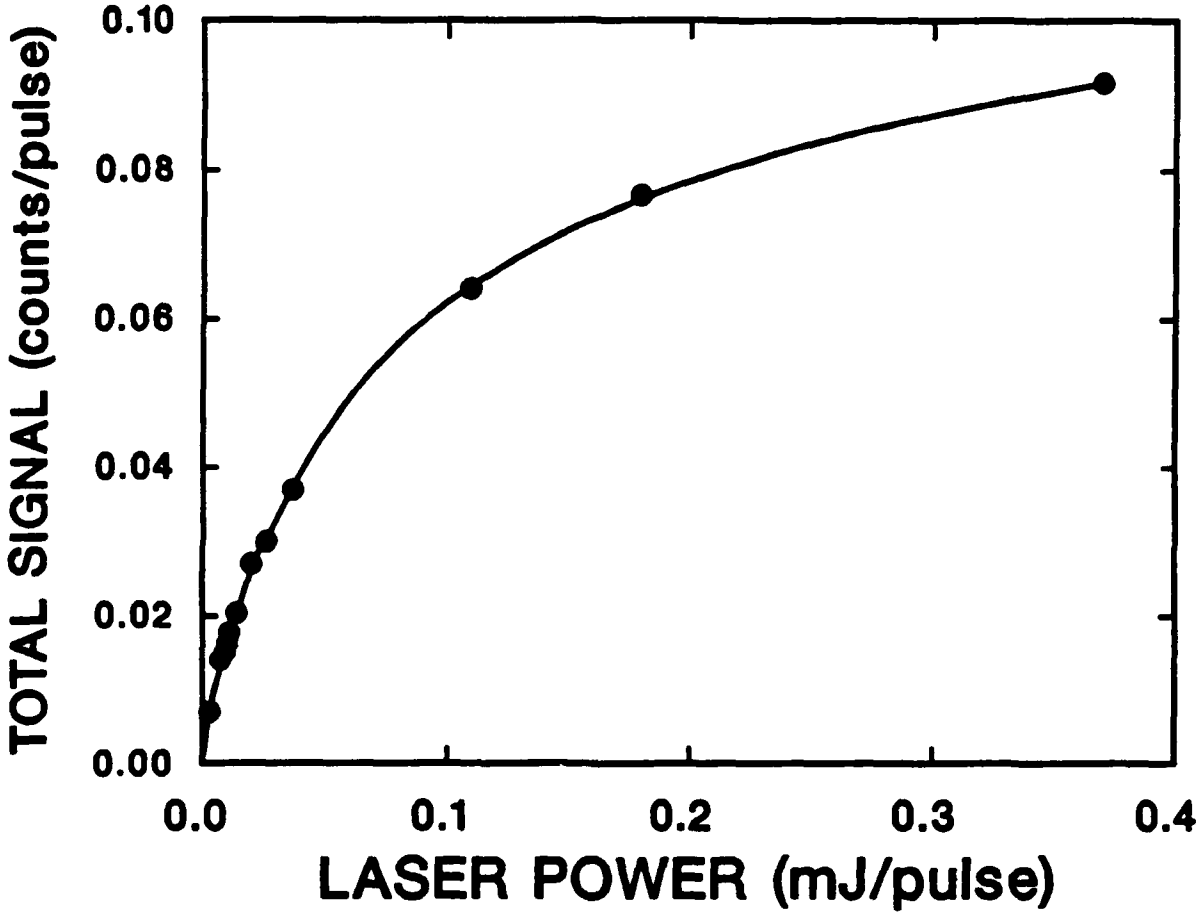

XBL 8811-3806

Fig 3

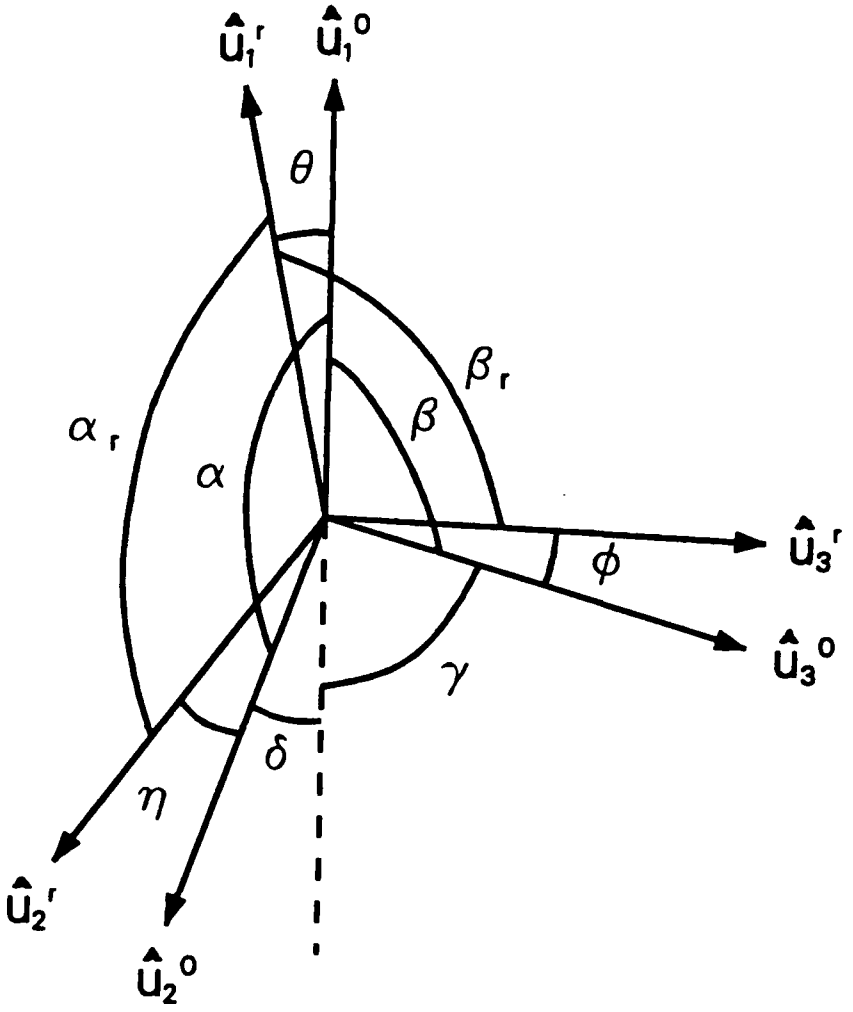

XBL 8811-3805

Fig 4

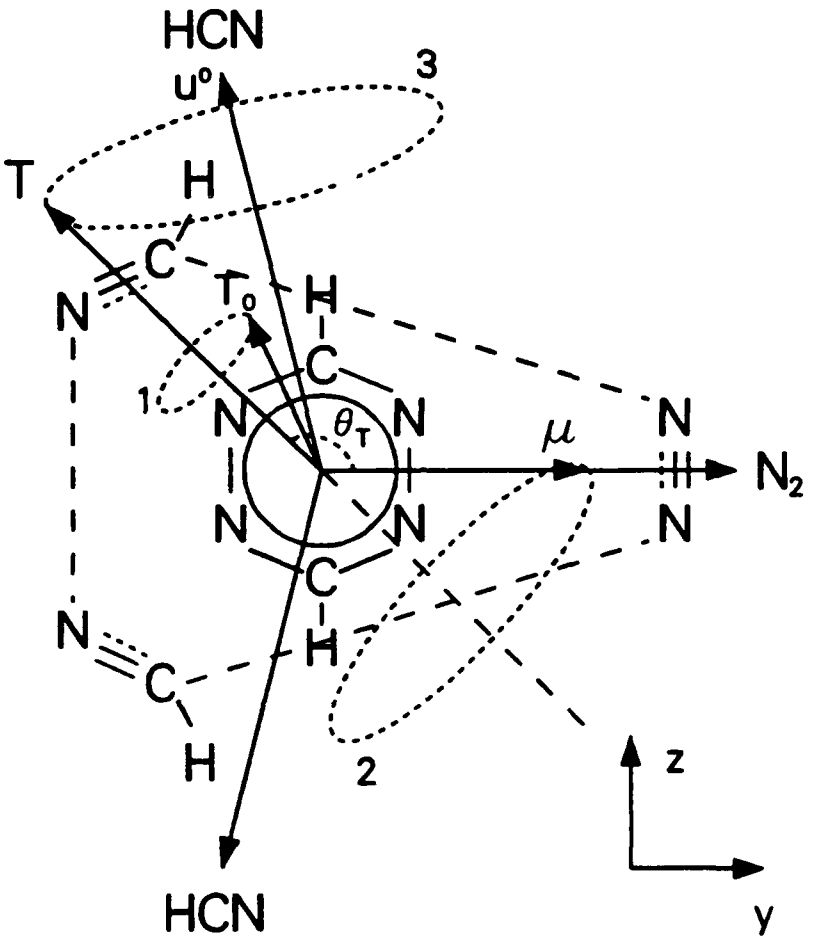

XBL 8811-3804

Fig 5

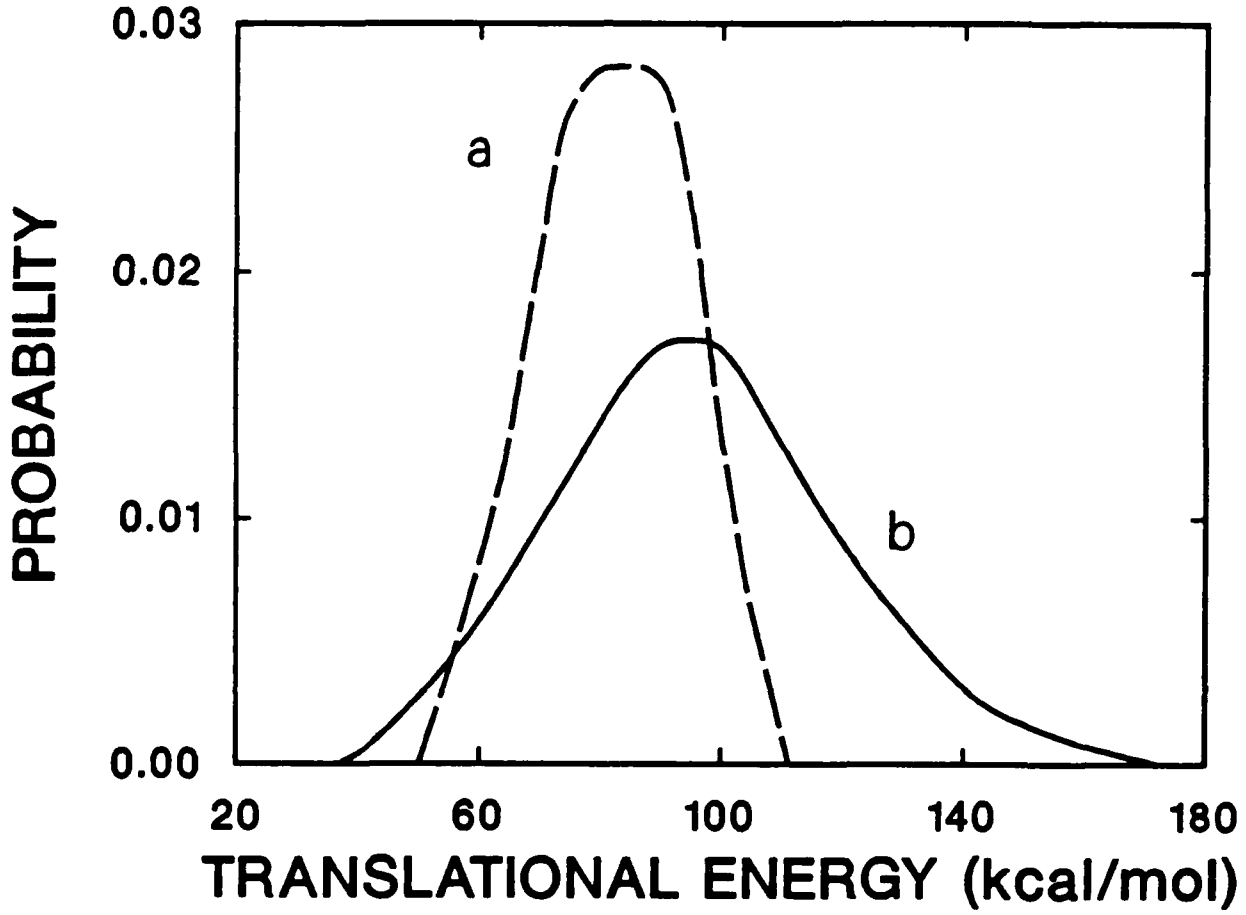

XBL 8811-3803

Fig 6

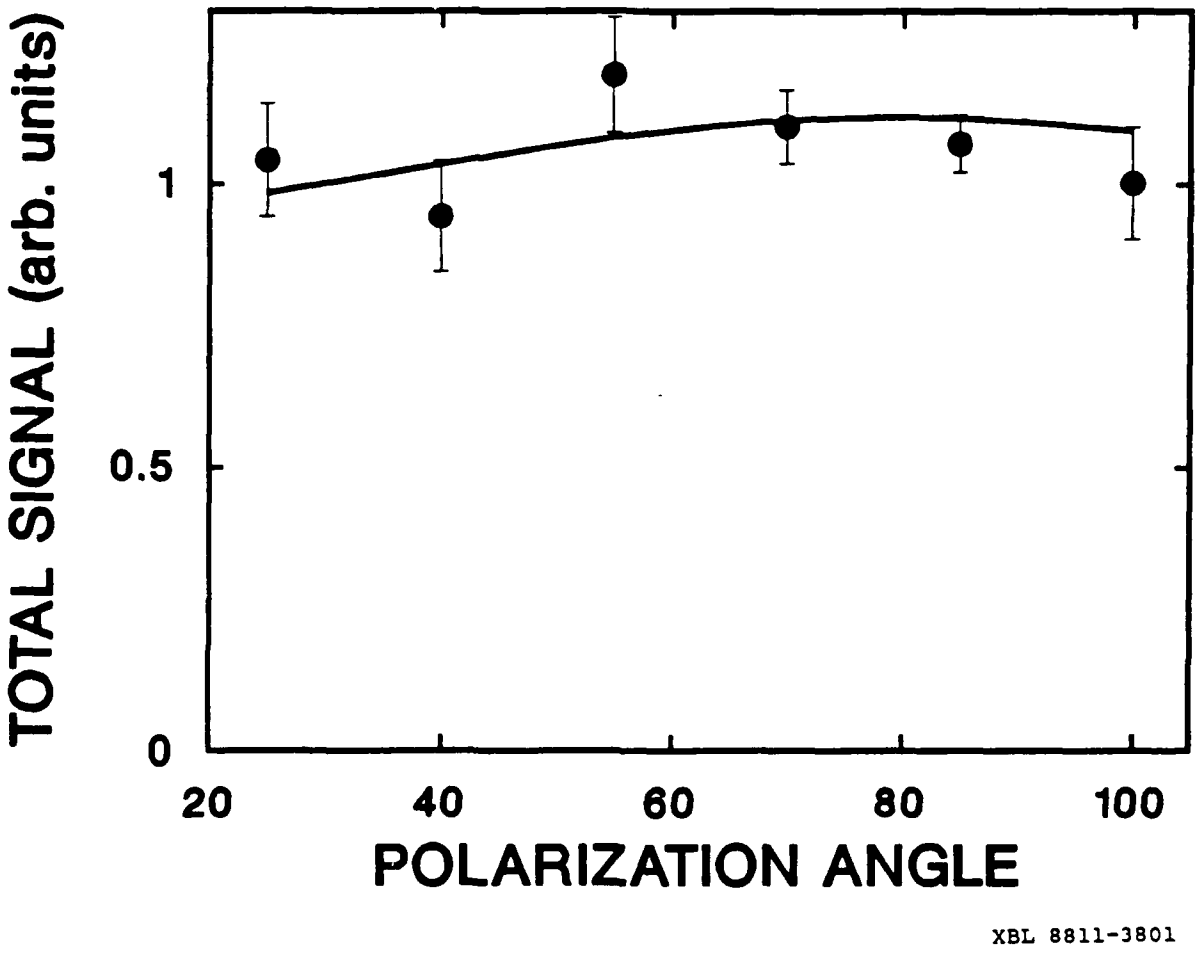

XBL 8811-3801

Fig 7

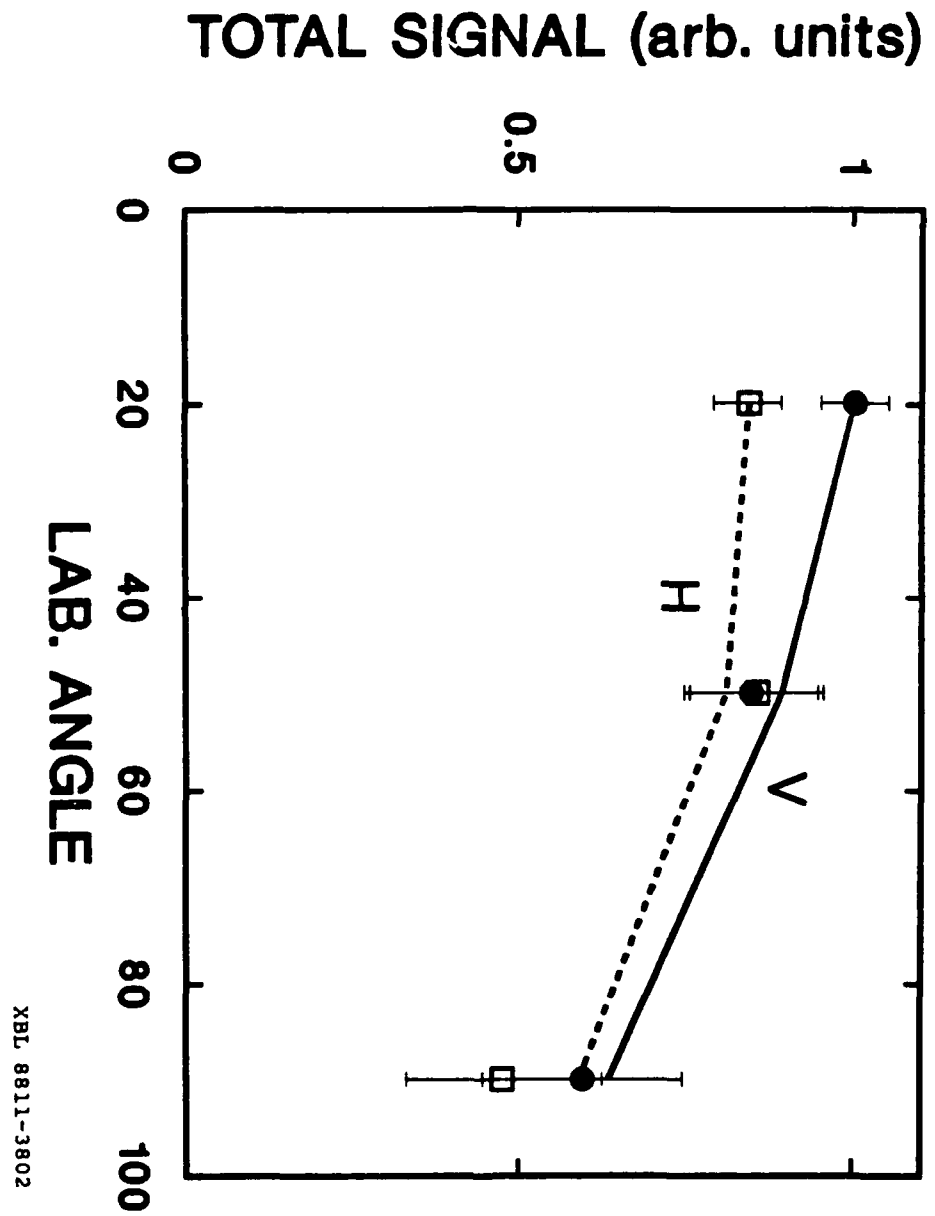
TOTAL SIGNAL (arb. units)
0
0.5
1
0
20
40
60
80
100
LAB. ANGLE
H
V
XBL 8811-3802

Fig 8

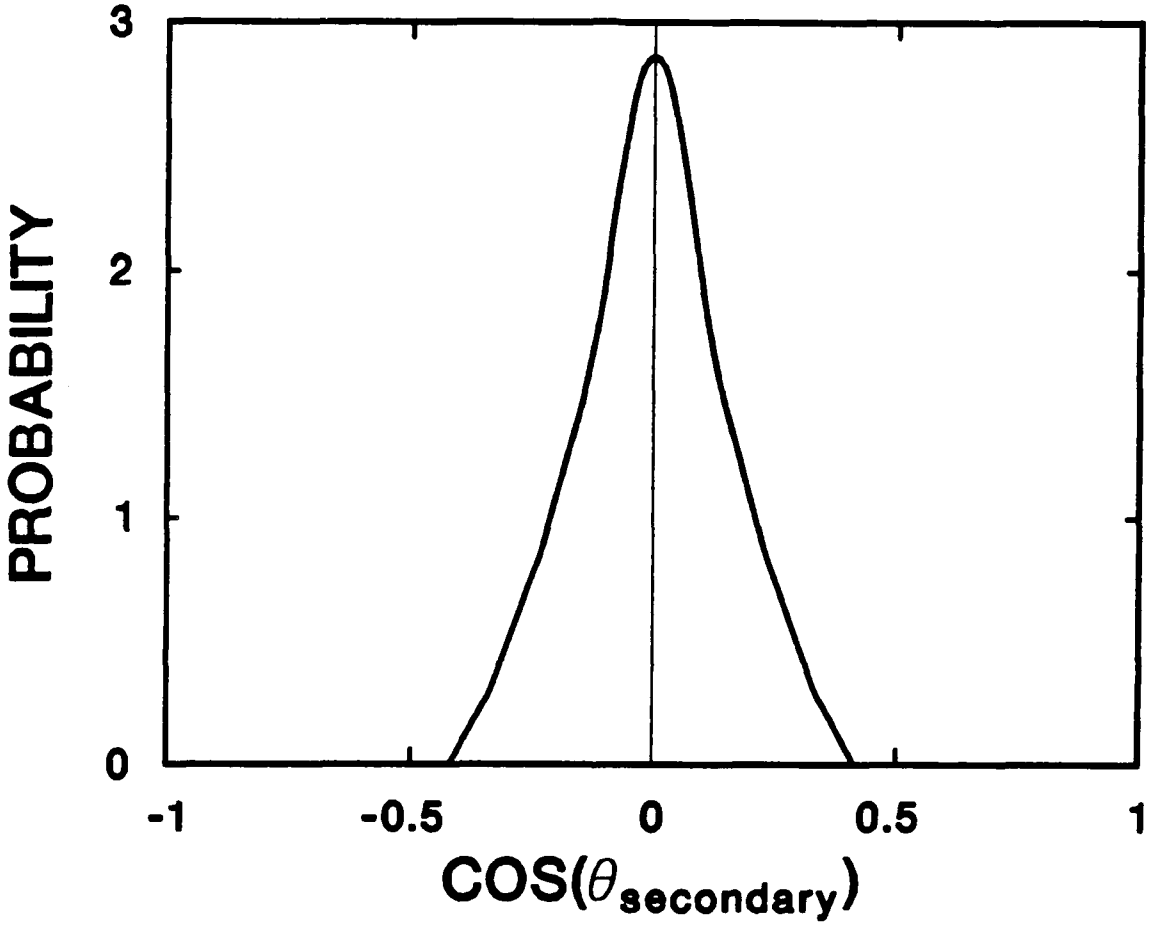

XBL 8811-3800

Fig. 9

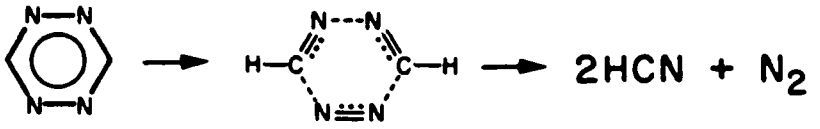

XBL 8811-3799

Reaction (3) in the text